Intermonomer Electron Transfer between the Low-Potential b Hemes of Cytochrome bc(1)

ARTICLE *in* BIOCHEMISTRY · FEBRUARY 2011

Impact Factor: 3.02 · DOI: 10.1021/bi101736v · Source: PubMed

BIOCHEMISTRY
including biophysical chemistry & molecular biology
Article

Biochemistry **2011,** *50,* 1651–1663 1651
DOI: 10.1021/bi101736v

Intermonomer Electron Transfer between the Low-Potential *b* Hemes of Cytochrome bc_1[†]

Pascal Lanciano, Dong-Woo Lee,[‡] Honghui Yang,[§] Elisabeth Darrouzet,[∥] and Fevzi Daldal*

Department of Biology, University of Pennsylvania, Philadelphia, Pennsylvania 19104, United States . [‡]Present address: Industrial Biotechnology and Bioenergy Research Center, Korea Research Institute of Bioscience and Biotechnology, Daejeon, Korea 305-806. [§]Present address: State Key Laboratory of Multiphase Flow in Power Engineering, Xi'an Jiaotong University, Xi'an 710049, China. [∥]Present address: CEA-iBEB, SBTN, Centre de Marcoule, Bat 170, BP17171, 30207 Bagnols sur Cèze, France.

Received October 28, 2010; Revised Manuscript Received January 19, 2011

ABSTRACT: Cytochrome (cyt) bc_1 is a structural dimer with its monomers consisting of the Fe-S protein, cyt *b*, and cyt c_1 subunits. Its three-dimensional architecture depicts it as a symmetrical homodimer, but the mobility of the head domain of the Fe-S protein indicates that the functional enzyme exists in asymmetrical heterodimeric conformations. Here, we report a new genetic system for studying intra- and intermonomer interactions within the cyt bc_1 using the facultative phototrophic bacterium *Rhodobacter capsulatus*. The system involves two different sets of independently expressed cyt bc_1 structural genes carried by two plasmids that are coharbored by a cell without its endogenous enzyme. Our results indicate that coexpressed cyt bc_1 subunits were matured, assorted, and assembled in vivo into homo- and heterodimeric enzymes that can bear different mutations in each monomer. Using the system, the occurrence of intermonomer electron transfer between the low-potential *b* hemes of cyt bc_1 was probed by choosing mutations that perturb electron transfer at the hydroquinone oxidation (Q_o) and quinone reduction (Q_i) sites of the enzyme. The data demonstrate that active heterodimeric variants, formed of monomers carrying mutations that abolish only one of the two (Q_o or Q_i) active sites of each monomer, are produced, and they support photosynthetic growth of *R. capsulatus*. Detailed analyses of the physicochemical properties of membranes of these mutants, as well as purified homo- and heterodimeric cyt bc_1 preparations, demonstrated that efficient and productive electron transfer occurs between the low-potential b_L hemes of the monomers in a heterodimeric enzyme. Overall findings are discussed with respect to intra- and intermonomer interactions that take place during the catalytic turnover of cyt bc_1.

The ubihydroquinone:cytochrome (cyt) *c* oxidoreductase (also called cyt bc_1[1] or complex III) is a major multisubunit membrane-bound enzyme that is central to respiratory and photosynthetic energy transduction pathways in various organisms (*1*). It converts hydroquinones (QH_2) to quinones (Q), reduces electron carrier cyt *c* forms, and contributes to the formation of membrane potential and proton gradient that are used for ATP production by ATP synthase (*2*, *3*). In most bacteria, like the purple non-sulfur phototroph *Rhodobacter capsulatus*, cyt bc_1 consists of three subunits (the Fe-S protein, cyt *b*, and cyt c_1), which are encoded by three structural genes, *petA*, *petB*, and *petC*, respectively (*4*), located adjacent to each other to form the *petABC* operon (*5*). Cyt *b* is an integral membrane protein, whereas the Fe-S protein and cyt c_1 are membrane-anchored by their amino- and carboxyl-terminal helices, respectively. These subunits are universally conserved in all cyt bc_1 forms and always carry specific cofactors essential for enzyme activity. These cofactors are the [2Fe-2S] cluster with a high redox midpoint potential (E_m) in the Fe-S protein, two *b*-type hemes with one low (b_L) and one high (b_H) E_m in cyt *b*, and a high-E_m *c*-type heme in cyt c_1 (*6*). The purified native *R. capsulatus* cyt bc_1 is a dimer but can also form tetramers upon fusion with one of its physiological electron carriers, the membrane-anchored cyt c_y (*7*). Each monomer of the enzyme contains two Q/QH_2 binding domains, termed the QH_2 oxidation (Q_o) and Q reduction (Q_i) sites, located on the positive (p) and negative (n) sides, respectively, of energy-transducing membranes. Three-dimensional structures for the cyt bc_1 forms of various organisms (including *R. capsulatus*) are known and often depict the enzyme as a symmetrical homodimer (*8*−*11*) (Figure 1). In each monomer (e.g., M1), the carboxyl-terminal helix of cyt c_1 interacts with the fifth helix of cyt *b* to form a cyt bc_1 core that interacts with only the head domain of the Fe-S protein, leaving the amino-terminal membrane helix of this subunit associated with cyt *b* of the other monomer (e.g., M2). The Fe-S protein head domain is mobile between cyt *b* and cyt c_1, and this mobility is essential for cyt bc_1 activity (*12*) as mutants with immobile Fe-S protein head domains are inactive (*13*). How the subunits are assembled to yield a functional enzyme is not well-established. Earlier works using *R. capsulatus* indicated that among the subunits and subcomplexes, the cyt c_1 subunit and the cyt bc_1 subcomplex are the longest-lived in vivo (*14*, *15*). These observations suggested that

[†]This work was supported by grants from the National Institutes of Health (R01 GM 38237) and the U.S. Department of Energy (91ER 20052) to F.D.

*To whom correspondence should be addressed. Telephone: (215) 898-4394. Fax: (215) 898-8780. E-mail: fdaldal@sas.upenn.edu.

[1]Abbreviations: cyt bc_1, ubihydroquinone:cytochrome *c* oxidoreductase; EPR, electron paramagnetic resonance; Fe-S, iron-sulfur; Q_o, hydroquinone oxidation; Q_i, quinone reduction; SQ, semiquinone; Ant, antimycin A; Myx, myxothiazol; Stig, stigmatellin; MPYE, mineral-peptone-yeast-extract; QH_2, hydroquinone; Q, quinone; MOPS, 4-morpholinepropanesulfonic acid; DBH_2, decylbenzohydroquinone; Flag, FLAG epitope; Strep, StrepTactin epitope.

Published on Web 01/24/2011

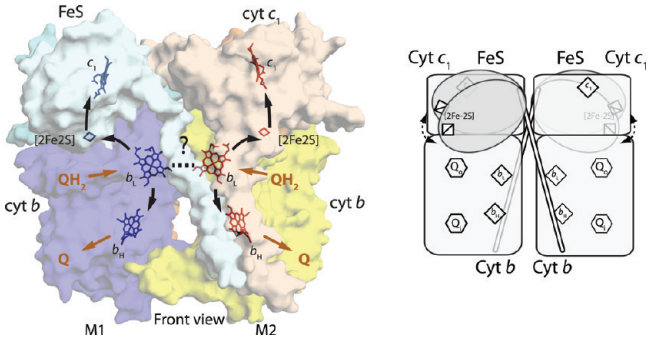

FIGURE 1: Three-dimensional structure of dimeric cyt bc_1 and its cofactors. The three-dimensional structure (Protein Data Bank entry 1ZRT for *R. capsulatus*) (left) of cyt bc_1 depicts it as a dimeric enzyme with two identical monomers, M1 and M2, each consisting of the Fe-S protein (light blue), cyt *b* (dark blue in M1 and yellow in M2), and cyt c_1 (beige). The figure was generated using Pymol (DeLano Scientific, San Carlos, CA), and the cofactors of each monomer ([2Fe-2S] cluster, hemes b_L and b_H, and c_1) are shown in different colors (blue in M1 and red in M2). Black and red arrows denote the electron transfer pathways between the cofactors and the Q_o and Q_i active sites of cyt bc_1, respectively. The intermonomer heme b_L–b_L distance is indicated with a dotted line, but for the sake of clarity, the distances (*11*) separating the cofactors are not shown. The right panel shows a schematic depiction of a homodimeric cyt bc_1, with its cofactors and Q_o and Q_i active sites, as described for the left panel.

first cyt *b* and c_1 might assemble together to which the Fe-S protein is added, but how and when the monomers form a dimer remains unknown. Related subcomplexes, probably representing assembly intermediates of cyt bc_1, have also been observed with yeast mitochondria (*16*).

The mechanism of function of cyt bc_1 is generally described by the Q cycle model (*17*) (see also ref *18*). At the Q_o site, the oxidized [2Fe-2S] cluster of the Fe-S protein oxidizes QH_2 and conveys one of the two electrons emanating from QH_2 oxidation to oxidized cyt c_1 via the mobility of the Fe-S protein head domain. cyt c_1 then reduces another cyt *c* (in *R. capsulatus*, cyt c_y or cyt c_2), which transports electrons to the photochemical reaction center (RC) in photosynthesis (Ps) or the cyt *c* oxidase in respiration (Res). The second electron derived from QH_2 oxidation at the Q_o site is transferred to heme b_L of cyt *b* and is then conveyed to heme b_H across the lipid bilayer, to generate membrane potential and yield a stable semiquinone (SQ) at the Q_i site. Completion of the catalytic turnover of cyt bc_1 involves a second QH_2 oxidation at a Q_o site, which proceeds via the same sequence of events described above but converting SQ in the Q_i site to a QH_2 to be released from the enzyme (Figure 1). Whether the same Q_o site of a given monomer, or the Q_o site at the other monomer of the dimeric enzyme, catalyzes this second QH_2 oxidation is unknown. In the past, models describing the mechanism of function of cyt bc_1 using dimeric enzymes have been proposed (*19*, *20*) (see also ref *21*). Recent experimental data stemming from crystallography (*22*), enzyme kinetics (*23*, *24*), and spectroscopy (*25*) suggest that intra- and intermonomer interactions occur in cyt bc_1, and that during the catalytic cycle the enzyme might become asymmetrical. The functional significance of any heterodimeric asymmetry remains unknown.

Our earlier works indicated that the presence of different Q_i site inhibitors affected the position of the Fe-S protein at the Q_o site across the membrane to initiate QH_2 oxidation (*25*). These intra- and intermonomer interactions led us to propose a "heterodimeric modified Q cycle" model (*26*). Accordingly, the resting enzyme would initiate a turnover at the Q_o site of any monomer but then alternate between the Q_o sites of the two monomers to complete the initiated turnover. This model follows the Q cycle events (*27*, *28*). In addition, it invokes intermonomer electron transfer between the b_L hemes of cyt *b* in each monomer to "dismutate" the two SQs accumulated at the distant Q_i sites of the dimeric enzyme to Q and QH_2 (*26*). More recent works indicated the occurrence of such electron transfer events (*29*, *30*). To further probe our model, we sought approaches to studying homo- and heterodimeric interactions between the monomers of cyt bc_1. Here we describe a new genetic system that allows modifications at will of cyt bc_1 subunits to induce structural asymmetry between monomers and yields architecturally heterodimeric enzymes. Successful production of heterodimeric cyt bc_1 forms indicates that the enzyme subunits were matured, assorted, and assembled independently in *R. capsulatus* membranes. Using this system, we initiated dissection of intra- and intermonomer interactions within the dimeric cyt bc_1 and describe a nativelike heterodimeric enzyme that exhibits fast and efficient electron transfer between the b_L hemes of the monomers to support cyt bc_1-dependent photosynthetic growth of *R. capsulatus*. Overall findings are discussed in terms of the biogenesis and mechanism of function of cyt bc_1 in the context of the heterodimeric modified Q cycle model.

MATERIALS AND METHODS

Bacterial Strains and Growth Conditions. All *R. capsulatus* strains harboring plasmids that express cyt bc_1 mutants were derivatives of strain MT-RBC1 [Δ(*petABC::spe*)] carrying a complete chromosomal deletion of *petABC* (*5*). They were grown in liquid or solid enriched (MPYE) medium, supplemented with antibiotics as needed (10 μg/mL kanamycin, 2.5 μg/mL tetracycline, or 10 μg/mL spectinomycin) under Res (semiaerobic/dark) or Ps (photoheterotrophic/light) conditions at 35 °C as described in ref *4*. For Ps growth, completely filled culture vessels or plates placed in anaerobic jars with H_2- and CO_2-generating gas packs (Becton Dickinson) were incubated in temperature-controlled Percival light incubators.

Escherichia coli strains harboring the plasmids used in this work (Table 1) were derivatives of HB101 [F^- Δ(*gpt-proA*)*62 araC14 leuB6*(Am) *glnV44*(AS) *galK2*(Oc) *lacY1* Δ(*mcrC-mrr*) *rpsL20*(Str^r) *xylA5 mtl-1 thi-1*] and grown on Luria-Bertani medium containing ampicillin, kanamycin, or tetracycline (100, 50, or 12.5 μg/mL, respectively) as appropriate (*4*). *R. capsulatus* strains harboring a single plasmid, or coharboring two plasmids with the same type of replicon or different (*inc*Q/P4 or *col*E1) types of replicons, were obtained via triparental matings between appropriate *E. coli* strains as donors and *R. capsulatus* strain MT-RBC1 as a recipient, as described previously (*5*). Depending on the replicon used, the desired plasmids were introduced by either conjugation or transformation, and either stepwise or simultaneously, using appropriate selections. Strains coharboring two plasmids were maintained using both antibiotics, and large cultures were subjected to short growth periods (~24 h). Under these conditions, cells harboring single or double plasmids produced Ps^+ revertants at frequencies of $< 10^{-5}$, and cultures that occasionally yielded larger numbers of Ps^+ revertants ($> 0.01\%$) were discarded so that biochemical analyses would not be compromised.

Molecular Genetic Techniques. Molecular genetic techniques were performed using standard procedures (*31*). All constructs were verified using DNA sequencing, and sequence

Table 1: Characteristics of the Different Plasmids Used in This Work

name	mutation	tag[a]	replicon[b]	resistance[a]	ref
pMTS1	no	no	incQ/P4	Kan^R	*38*
pMTS1-S	no	S	incQ/P4	Kan^R	this work
pMTS1-F	no	F	incQ/P4	Kan^R	this work
pED2	*petB:Y147A* (Q_o site)	S	incQ/P4	Kan^R	this work
pED3	*petB:H212N* (Q_i site)	F	fused incQ/P4+colE1	Tet^R	this work
pHY101	*petB:H212N* (Q_i site)	F	incQ/P4	Tet^R	this work
pHY103	*petB:Y147A* (Q_o site)	S	fused incQ/P4+colE1	Kan^R	this work

[a] *petB* is carboxyl-terminally epitope-tagged with S (StrepTactin) or F (FLAG) tags as indicated, and Kan^R and Tet^R refer to kanamycin and tetracycline resistance, respectively. [b] incQ/P4 and fused incQ/P4+colE1 refer to pRK-type and composite-type plasmids, respectively.

analyses were conducted using MacVector (Accelrys, San Diego, CA). Carboxyl-terminally epitope-tagged derivatives of cyt *b* were constructed using the "QuickChange Site-Directed Mutagenesis kit" (Stratagene, La Jolla, CA), with plasmid pPET1 carrying the wild-type *petABC* operon (*5*) as a template, and the primer pairs of FlagF1 (5′-TCCGGCCGAG**GACTACAAGGACGACGACGACAAG**TGAGGAAAGGAACCG-3′) and FlagR1 (5′-CCTTTCCTCA**CTTGTCGTCGTCGTCCTTGTAGTC**CTCGGCCGGATTGCCG-3′) encoding the Flag (-**DYKDDDDK**-COOH) (F) tag, StrepF1 (5′-TCCGGCCGAG**TGGTCGCACCCGCAGTTCGAAAAG**TGAGGAAAGGAACCG-3′) and StrepR1 (5′-CCTTTCCTCA**CTTTTCGAACTGCGGGTGCGACCA**CTCGGCCGGATTGCCG-3′) encoding the Strep (-**WSHPQFEK**-COOH) (S) tag, HAF1 (5′-TCCGGCCGAG-**TACCCGTACGACGTCCCGGACTACGCGT**GAGGAAAGGAACCG-3′) and HAR1 (5′-CCTTTCCTCA**CGCGTAGTCCGGGACGTCGTACGGGTA**CTCGGCCGGATTGCCG-3′) encoding the HA (-**YPYDVPDYA**-COOH) (H) tag, or cMycF1 (5′-TCCGGCCGAG**GAGCAGAAGCTTATCTCGGAGGAGGACCTGT**GAGGAAAGGAACCG-3′) and cMycR1 (5′-CCTTTCCTCA**CAGGTCCTCCTCCGAGATAAGCTTCTGCTC**CTCGGCCGGATTGCCG-3′) encoding the cMyc (-**EQKLISEEDL**-COOH) (M) tag, yielding plasmids pPET1-F, pPET1-S, pPET1-H, and pPET1-M, respectively. The *Xma*I−*Stu*I fragment of pMTS1 was then exchanged with its counterparts from appropriately tagged plasmid pPET1 derivatives to yield pMTS1-F, pMTS1-S, pMTS1-H, and pMTS1-M (Table 1). Similarly, pED2 (Kan^R) carrying a mutant allele of *petABC* with a cyt *b*-S:Y147A mutation that inactivates Q_o site electron transfer was obtained by exchanging the *Xma*I−*Stu*I fragments between pPET1-S and pMTS1-*b*:Y147A plasmids (*32*). Plasmid pPET1-H212N* was obtained by exchanging the *Sty*I−*Sph*I fragments between pPET1-F and pPET1-H212N plasmids, and then the *BstE*II fragment carrying the cyt *b*-F:H212N mutation of pPET1-H212N* was substituted with that of pRKpPET1-bH212N (*28*) to yield pED3 (Tet^R). To construct plasmid pHY101, which is a pRK415 Tet^R derivative carrying a mutant *petABC* with the cyt *b*-F:H212N mutation, pED3 was digested with *Hin*dIII, ligated, and transformed into HB101 selecting for Amp^R, to yield pHY100 that carries *petABC*. This plasmid was digested with *Tth*III, blunt ended with T4 polymerase, and digested with *Hin*dIII to generate a DNA fragment carrying *petABC* with the cyt *b*-F:H212N mutation, which was ligated to Tet^R plasmid pRK415 digested first with *Xba*I, blunt ended with T4 polymerase, and then digested with *Hin*dIII to yield pHY101 (Table 1). An Amp^R Tet^S derivative of plasmid pBR322 (*33*) was constructed by digestion with *Eco*RV and *Ava*I, religation, and transformation into HB101 to yield pHY102. Ligation of plasmids pHY102 and pED2 carrying *petABC* with the cyt *b*-S:Y147A mutation using their unique *Hin*dIII sites yielded plasmid pHY103. The characteristics of the plasmids used are summarized in Table 1.

Biochemical Techniques. Intracytoplasmic (chromatophore) membranes were obtained from frozen washed cells after two passes through a French pressure cell, as described previously (*5*). Protein concentrations were determined using the bicinchoninic acid method (*34*) with bovine serum albumin as a standard. Sodium dodecyl sulfate−polyacrylamide gel electrophoresis (SDS−PAGE) (12.5%) was conducted as described in ref *35*, and prior to being loaded, samples were solubilized by incubation for 10 min at room temperature in 62.5 mM Tris-HCl (pH 6.8), 2% SDS, 0.1 M dithiothreitol, 25% glycerol, and 0.01% bromophenol blue. Immunoblot analyses were conducted as described in ref *5* using polyclonal antibodies against *R. capsulatus* cyt *b*, or anti-Flag (Sigma Inc.) and anti-Strep antibodies (Novagen Inc.). Steady-state cyt bc_1 activity was measured using decylbenzohydroquinone (DBH_2) as an electron donor and horse heart cyt *c* as an electron acceptor at 25 °C (*5*). The reaction was initiated by enzyme addition and monitored at 550 nm for 2 min, and the portion of the initial rate that is sensitive to stigmatellin was taken as enzyme activity.

Spectroscopic Techniques. Optical spectra were recorded on a Hitachi U3210 UV−visible spectrophotometer. Absorption difference spectra for the *c*- and *b*-type cyts were obtained using chromatophore membranes (0.3 mg of total protein/mL), oxidized with potassium ferricyanide, and reduced with sodium ascorbate or sodium dithionite, as appropriate. Potentiometric dark titrations using optical or EPR spectra were performed with chromatophore membranes (1.5 or 10 mg/mL, respectively) or purified cyt bc_1 (0.5 mg/mL) preparations, as described previously (*36*). A buffer [50 mM MOPS and 100 mM KCl (pH 7.0)] containing 20 μM tetrachlorohydroquinone [TCHQ ($E_{m,7}$ = 350 mV)], 20 μM 2,3,5,6-tetramethyl-1,4-phenylenediamine [DAD (260 mV)], 20 μM 1,2-naphthoquinone 4-sulfonate [NQS (210 mV)], 20 μM 1,2-naphthoquinone [NQ (145 mV)], 10 μM *N*-methyldibenzopyrazine methyl sulfate [PMS (80 mV)], 10 μM *N*-ethyldibenzopyrazine methyl sulfate [PES (50 mV)], 40 μM duroquinone [DQ (5 mV)], 20 μM pyocyanine [PCN (−34 mV)], 6 μM indigo trisulfonate [ITS (−90 mV)], 20 μM 2-hydroxy-1,4-naphthoquinone [HNQ (−145 mV)], and 20 μM anthraquinone 2-sulfonate [AQS (−225 mV)] as redox mediators was used. The optical changes that accompanied the E_h changes were recorded in the α-band region (500−600 nm), and the E_m values were determined by fitting the normalized absorption data to appropriate numbers of components $n = 1$ Nernst equation. The mediator cocktail was tested for the absence of any optical absorbance contribution during the titrations. EPR measurements were taken on a Bruker Elexsys E500 spectrometer. X-Band EPR spectra were recorded using a standard rectangular Bruker cavity (ER 4102ST)

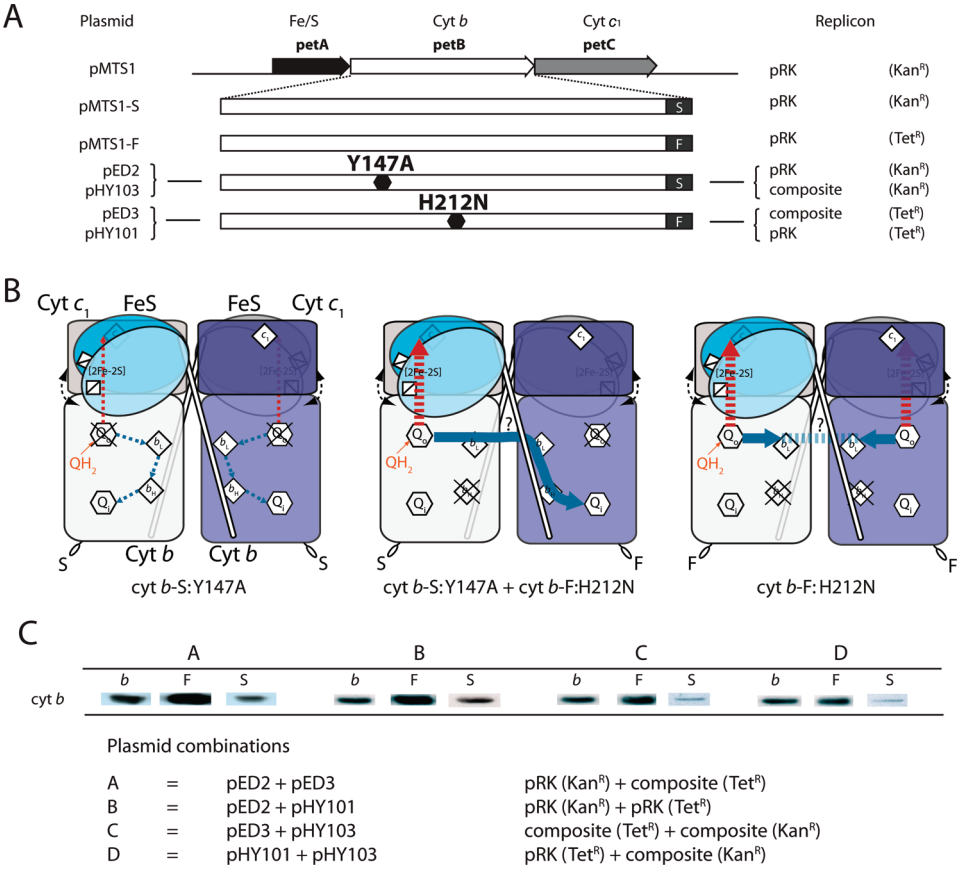

FIGURE 2: Genetic system for studying intra- and intermonomer interactions in the cyt bc_1 dimer: cyt *b*-S:Y147A−cyt *b*-F:H212N heterodimeric cyt bc_1 variant in *R. capsulatus*. (A) The different plasmids carrying the *petABC* operon (left), their replicon type and antibiotic resistance markers (right), and the location of cyt *b* mutations in *pet*B (middle) that they carry are shown together with the Strep (S) and Flag (F) epitope tags added at the carboxyl-terminal end of cyt *b*. The brackets are to indicate that pED2 and pHY103 carry the same cyt *b* mutation but in two different replicons with the same antibotic resistance marker, and the same is also the case for pED3 and pHY101. (B) Coexpression of a Kan^R plasmid carrying the *petABC* operon with the cyt *b*-S:Y147A mutation and a Tet^R plasmid carrying the *petABC* operon with a cyt *b*-F:H212N mutation yields homodimeric cyt *b*-S:Y147A (left) and cyt *b*-F:H212N (right) as well as heterodimeric cyt *b*-S:Y147A−cyt *b*-F:H212N (middle) cyt bc_1 variants. The thin dotted arrows refer to residual electron transfer that occurs in the homodimeric cyt *b*-S:Y147A variant, whereas the thick red dashed arrows and thick blue solid arrows correspond to electron transfer to the high- and low-potential cofactors of cyt bc_1, respectively. Note that intermonomer heme b_L to b_L electron transfer is indicated by a thick blue solid arrow. (C) SDS−PAGE and immunoblot analyses of Strep- and Flag-tagged cyt *b* in chromatophore membranes of strains harboring different combinations of Kan^R and Tet^R plasmids (A−D, as indicated) producing heterodimeric cyt bc_1 variants. Approximately 10 μg of total proteins was used, and cyt *b* contents were determined using polyclonal antibodies specific to *R. capsulatus* cyt *b* (*b*) as well as commercially available antibodies against the Flag (F) and Strep (S) epitope tags. Properties of the plasmids used are described in Table 1.

fitted to an Oxford Instruments helium flow cryostat (ESR900). Spectrometer settings are listed in the figure legends.

Time-resolved, light-activated kinetic spectroscopy was performed on a dual-wavelength kinetic spectrophotometer with chromatophore membranes resuspended in 50 mM MOPS/100 mM KCl buffer (pH 7.0) supplemented with 100 μM ferricyanide [FeCN (430 mV)], 8 μM DAD (260 mV), 6 μM NQ (145 mV), 1 μM PMS (80 mV), 1 μM PES (50 mV), 6 μM 2 HNQ (−145 mV), and 6 μM benzyl viologen [BV (−359 mV)] as redox mediators and 2.5 μM valinomycin as a membrane potential uncoupler (*37*). The amounts of chromatophore membranes used in each assay were normalized to their reaction center (RC) content, as determined by measuring the flash-induced optical absorbance difference between 605 and 540 nm (E_h = 380 mV), and an extinction coefficient of 29.8 mM^{-1} cm^{-1}. Transient cyt *c* re-reduction and cyt *b* reduction kinetics at an E_h of 100 mV, initiated by a short saturating flash (~8 μs) from a xenon lamp, were followed at 550−540 and 560−570 nm, respectively. Antimycin, myxothiazol, and stigmatellin were used at 10 μM each, as needed.

Protein Purifications. *R. capsulatus* wild type, homo- or heterodimeric mutant, epitope-tagged, or untagged cyt bc_1 species were purified using appropriate derivatives of MT-RBC1 (Table 1). Washed chromatophore membranes were resuspended to a final protein concentration of 10 mg/mL in 50 mM Tris-HCl buffer (pH 8.0) containing 100 mM NaCl, 20% glycerol, and 1 mM PMSF. Dodecyl maltoside [DDM, 20% (w/v) stock solution] was added dropwise to a final concentration of 1 mg of detergent/mg of total protein. The mixture was stirred for 1 h at 4 °C and then ultracentrifuged (120000*g* for 1 h) to eliminate nondispersed membranes. The supernatant was loaded onto a DEAE-Biogel A column (5.2 cm × 15 cm) pre-equilibrated with 50 mM Tris-HCl (pH 8.0) containing 20% glycerol, 0.01% (w/v) DDM, and 100 mM NaCl (buffer A). The column was washed with 3 column volumes (CV) of buffer A, followed by 5 CV of the same buffer supplemented with 150 mM NaCl. With the cyt bc_1 variants derived from cells harboring pMTS1, pMTS1-S, pMTS1-F, and pED2, the column was washed stepwise between 150 and 350 mM NaCl until a red band adsorbed on top of the column became visible, which was then eluted with

350 mM NaCl. However, with the cyt bc_1 variant with the cyt *b*-F:H212N mutations produced by cells harboring pED3 or pED2+pED3, this red band started to elute at salt concentrations of >150 mM. In all cases, fractions were monitored for their absorption at 280 and 420 nm, and those with a reddish color, dithionite-reduced minus ferricyanide-oxidized optical difference spectra at 520−580 nm, were recorded. Fractions containing the highest concentrations of *c*- and *b*-type cyts were pooled, concentrated using an Amicon Diaflo apparatus equipped with a PM30 membrane, and stored at −80 °C. Concentrated cyt bc_1 preparations from cells carrying pMTS1-F or pED3 were passed twice through an anti-FLAG M2 affinity column (1 mL), pre-equilibrated with 15 CV of TBS [50 mM Tris-HCl buffer (pH 8.0) containing 150 mM NaCl, 20% glycerol, and 0.01% (w/v) DDM]. The column was washed with 10 CV of the same buffer and eluted with 6 CV of a solution containing 100 μg/mL FLAG peptide in TBS. Fractions containing cyt bc_1 were pooled, concentrated using Amicon Ultra (50000 M_r cutoff) centrifugal filter devices (Millipore Inc.), and stored at −80 °C in the presence of 20% glycerol until further use. In the case of cyt bc_1 variants derived from cells carrying pMTS1-S or pED2, concentrated samples were loaded twice onto a StrepTactin affinity column (1 mL) pre-equilibrated with 5 CV of TBS buffer. The column was washed with 10 CV of the same buffer and eluted with 6 × 0.5 CV of a solution containing 1 mM hydroxyazophenylbenzoic acid (HABA) in TBS. Fractions containing cyt bc_1 were pooled, concentrated using Amicon Ultra (50000 M_r cutoff) centrifugal filter devices (Millipore Inc.), and stored at −80 °C in the presence of 20% glycerol until further use. When affinity-purified cyt bc_1 samples were subjected to a second affinity chromatography using a different epitope (i.e., Flag to Strep or Strep to Flag), they were first concentrated and then processed as described above.

Chemicals. The cyt bc_1 inhibitors antimycin A, myxothiazol, and stigmatellin as well as duroquinone were purchased from Sigma Inc. Dodecyl maltoside was from Anatrace Inc., and DEAE-BioGel A was from Bio-Rad. All other chemicals were of reagent grade or of the highest quality commercially available.

RESULTS

A Genetic System for Studying Intra- and Intermonomer Interactions in cyt bc_1. A new genetic system that produces heterodimeric variants of cyt bc_1 was developed for studying intra- and intermonomer interactions in the *R. capsulatus* enzyme. In this system, alleles of *petA*, *petB*, and *petC* encoding cyt bc_1 subunits were carried by different plasmids marked with distinct antibiotic resistance markers (Kan^R and Tet^R) to ensure coselection (Figure 2A) and coexpressed in a strain devoid of its endogenous chromosomally encoded enzyme (*5*). We reasoned that coexpression of genetically distinct copies of cyt bc_1 structural genes might yield homodimeric and heterodimeric enzyme variants if the assembly and dimerization of different subunits occur randomly during cyt bc_1 biogenesis (Figure 2B). In addition, different epitope tags (Strep, Flag, HA, and cMyc) were added to the cyt *b* subunit of cyt bc_1 to physically distinguish the homo- and heterodimeric variants upon purification. Extension of the carboxyl-terminal end of a wild-type cyt *b* with any one of the four epitope-tags tested yielded functional cyt bc_1 variants that fully complemented for Ps growth a cyt bc_1^- strain of *R. capsulatus*. The Strep- and Flag-tagged cyt bc_1 derivatives were chosen for further experiments on the basis of their relative stabilities during subsequent purification procedures.

A Heterodimeric cyt bc_1 for Probing Intermonomer Electron Transfer between Its b_L Hemes. A heterodimeric cyt bc_1, with one inactive Q_i site in one monomer and one inactive Q_o site in the other monomer, was sought to investigate intermonomer electron transfer between the two b_L hemes of cyt bc_1 (Figure 2B). Earlier, we had reported that the cyt *b*:Y147A mutation abolishes the transfer of an electron from oxidized QH_2 to heme b_L without affecting the binding of Q or QH_2 to the Q_o site, the transfer of an electron from heme b_L to b_H (*32*), or the mobility of the Fe-S protein head domain between cyt *b* and cyt c_1 (*12*). Similarly, we had found that the cyt *b*:H212N mutation caused a loss of heme b_H without prohibiting enzyme assembly but enhanced the Fe-S protein head domain mobility at the Q_o site by decreasing intra- and intermonomer regulatory controls (*25*). These two mutations together with the Flag and Strep tags were used to produce "two-Q_o site defective homodimer" (cyt *b*-S:Y147A−cyt *b*-S:Y147A), "two-Q_i site defective homodimer" (cyt *b*-F:H212N−cyt *b*-F:H212N), and "one-Q_o site, one-Q_i site defective heterodimer" (cyt *b*-S:Y147A−cyt *b*-F:H212N) cyt bc_1 variants (Figure 2B). Moreover, earlier works indicated that the amounts of membrane proteins produced in *R. capsulatus* cells under different growth conditions depend on the plasmids used. A broad host-range plasmid of the pRK type (i.e., pMTS1) overproduced cyt bc_1, whereas a "composite" plasmid (i.e., pMTS0) obtained by fusing a pRK-type plasmid (i.e., pRK404) with a ColE1-type plasmid (i.e., pPET1) yielded variable levels of overproduction in different cases (*5*, *38*). Thus, variants with cyt *b*-S:Y147A and cyt *b*-F:H212N substitutions carried by pRK-type (Kan^R pED2 and Tet^R pHY101, respectively) or composite (Kan^R pHY103 and Tet^R pED3, respectively) plasmids were constructed (Table 1), were conjugated into a cyt bc_1^- mutant under Res growth conditions using appropriate Kan^R and Tet^R selections, and yielded cells harboring one or two different kinds of plasmids and producing homo- and heterodimeric cyt bc_1 variants.

Characterization of R. capsulatus Strains Producing Homo- and Heterodimeric cyt bc_1 Variants. *R. capsulatus* strains harboring a single plasmid with wild-type *petABC* (pMTS1, pMTS1-S, and pMTS1-F) were Ps^+, and those with mutant *petABC* (pED2, pED3, pHY101, and pHY103) were Ps^- (Figure 3A). Interestingly, cells harboring two plasmids in any of the four combinations tested (A, pED2 and pED3; B, pED2 and pHY101; C, pHY103 and pED3; and D, pHY103 and pHY101) exhibited slow Ps (i.e., $Ps^{\pm}$) growth (Table 2), suggesting that concurrent expression of genetically distinct *petABC* operons yielded functional heterodimeric cyt bc_1 variants, which is a prerequisite for Ps growth of *R. capsulatus*. Indeed, use of SDS−PAGE and immunoblots with antibodies against cyt *b* as well as the Strep or Flag epitopes indicated that chromatophore membranes from the two plasmids harboring cells grown under Res conditions contained both Strep- or Flag-tagged cyt bc_1 variants (Figure 2C). Semiquantitative estimations suggested that among the four combinations, those containing two pRK-type (pED2 and pHY101) or two composite (pHY103 and pED3) plasmids produced comparable amounts of Strep- or Flag-tagged cyt *b* variants and revealed that this subunit was mature and assorted independently during cyt bc_1 biogenesis. Cells harboring pED2 and pED3 (combination A, cyt *b*-S:Y147A and cyt *b*-F:H212N) were retained for further studies. Under Ps growth conditions, cells harboring pED2 and pED3 formed

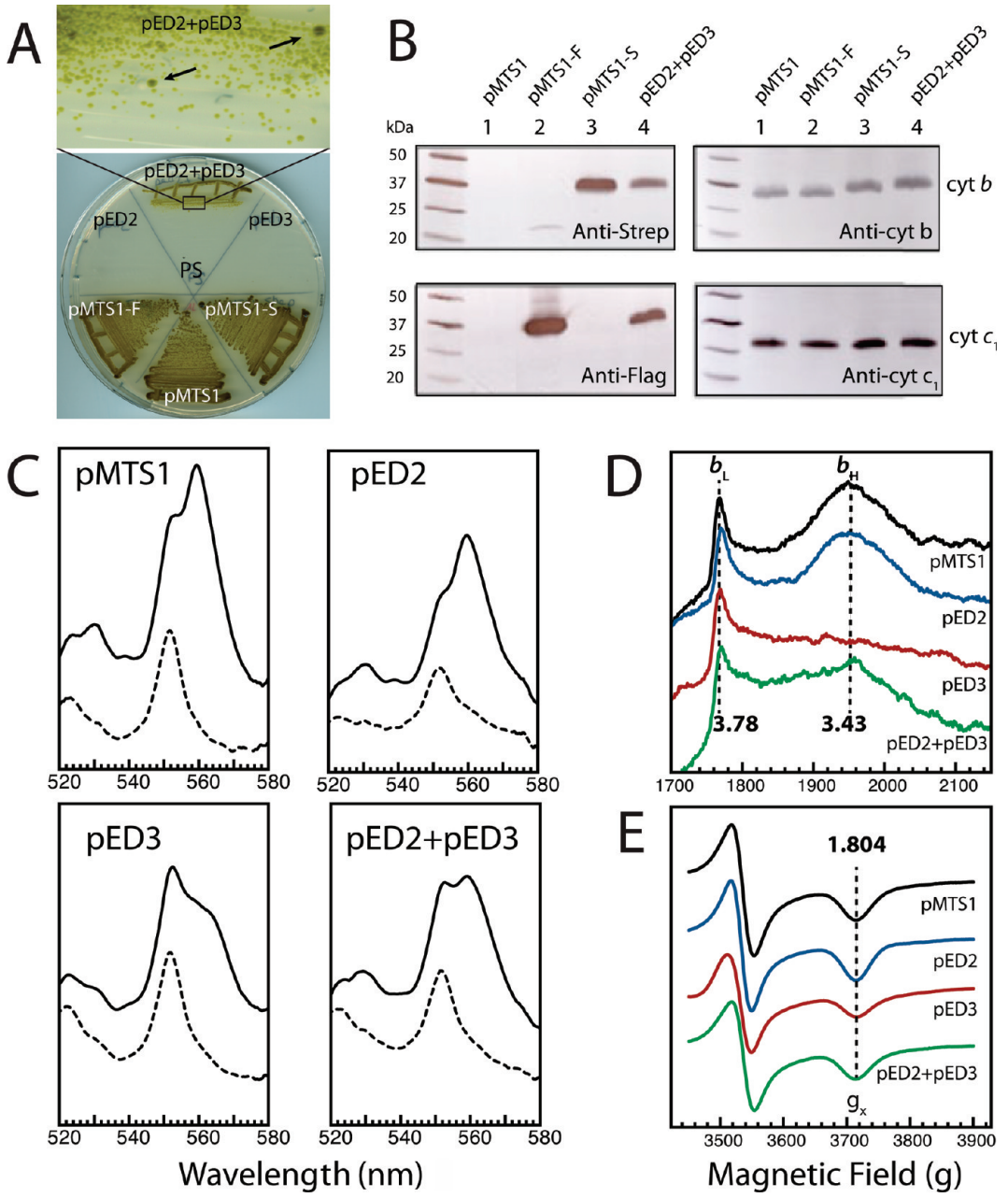

FIGURE 3: Photosynthetic growth phenotypes and biochemical properties of *R. capsulatus* strains producing heterodimeric cyt bc_1 variants. (A) Photosynthetic (Ps) growth on enriched medium of *R. capsulatus* strains harboring plasmids pMTS1, pMTS1-S, and pMTS1-F producing wild type, pED2+pED3 producing homodimeric cyt *b*-S:Y147A and cyt *b*-F:H212N, and pED2+pED3 producing heterodimeric cyt *b*-S:Y147A and cyt *b*-F:H212N cyt bc_1 variants. Cells harboring pMTS1, pMTS1-S, and pMTS1-F are Ps^+; those harboring pED2 or pED3 are Ps^-, and those harboring both pED2+pED3 are $Ps^{\pm}$ (i.e., slow growth). Shown above the plate a small section in which rare Ps^+ revertants in pED2−pED3 cultures (indicated by arrows) are observed. (B) Chromatophore membranes of appropriate *R. capsulatus* strains described in panel A and grown by respiration in enriched medium were analyzed by SDS−PAGE (15%) and immunoblots using approximately 10 μg of total proteins. The cyt *b* and cyt c_1 subunits were determined using polyclonal anti-cyt *b* or anti-cyt c_1 (right) or anti-Strep II and anti-Flag M2 (left) antibodies as indicated. (C) Total *b*-type and *c*-type cyt content of chromatophore membranes (0.3 mg/mL) obtained from appropriate *R. capsulatus* strains (as described for panel A) grown by respiration in enriched medium determined by ascorbate (---) or dithionite (—) reduced minus ferricyanide oxidized optical difference spectra. Note the differences seen between the stains harboring different plasmids and producing different cyt bc_1 variants. (D) Low-spin heme EPR spectra from redox-poised chromatophore membranes obtained from appropriate *R. capsulatus* strains (as described for panel A) grown by respiration in enriched medium. The ambient redox potential (E_h) values at which the spectra were recorded were 255, 260, 300, and 290 mV for membranes derived from cells harboring pMTS1, pED2, pED3, and pED2+pED3 plasmids, respectively. The following experimental conditions were used: temperature, 10 K; microwave power, 10 mW at 9.420 GHz; modulation amplitude, 10 G at 100 kHz; and four scans. Note that no baseline correction was used. (E) [2Fe-2S] EPR spectra of redox-poised chromatophore membranes obtained from appropriate *R. capsulatus* strains (as described for panel A) grown by respiration in enriched medium. The E_h values at which the spectra were recorded were 123, 112, 116, and 126 mV for membranes derived from cells harboring pMTS1, pED2, pED3, and pED2+pED3 plasmids, respectively. The following experimental conditions were used: temperature, 20 K; microwave power, 2 mW at 9.416 GHz; modulation amplitude, 20 G at 100 kHz; one scan.

smaller colonies than a wild-type strain, suggesting that they exhibited lower than normal levels of cyt bc_1 activity, while those containing either pED2 or pED3 remained Ps^- (Figure 3A). Cells harboring either pED2 or pED3, or both pED2 and pED3,

Table 2: Characteristics of Various Homo- and Heterodimeric cyt bc_1 Variants

strain	Ps growth[a]	b/c ratio[b]	DBH_2 activity[c] (%)	$E_{m,7}$[d] (mV)			dimer assembly[e]	
				b_L	b_H	c_1	homo	hetero
pMTS1	+	1.6	100	−133	67	310	−	
pMTS1-S	+	1.6	106	nd[g]	nd[g]	nd[g]	SS	
pMTS1-F	+	1.7	80	nd[g]	nd[g]	nd[g]	FF	
pED2	−	1.7	13.2[f]	−137	70	305	SS	
pHY103	−	nd[g]	nd[g]	nd[g]	nd[g]	nd[g]	SS	
pED3	−	0.5	9.2[f]	−145	na[h]	300	FF	
pHY101	−	nd[g]	nd[g]	nd[g]	nd[g]	nd[g]	FF	
pED2+pED3 (A)	±	0.9	22	−147	73	300		FF+SS+FS
pED2+pH101 (B)	±	1	19	nd[g]	nd[g]	nd[g]		FF+SS+FS
pED3+pHY103 (C)	±	0.75	17.5	nd[g]	nd[g]	nd[g]		FF+SS+FS
pH101+pHY103 (D)	±	0.65	15	nd[g]	nd[g]	nd[g]		FF+SS+FS

[a]Ps refers to photosynthetic growth, and +, −, and ± denote vigorous, no, and slow growth ability, respectively. [b]b/c ratio refers to the cyt b/cyt c ratio determined by optical difference spectroscopy using membranes as described in Materials and Methods. [c]DBH_2 activity indicates the amount of DBH_2:cyt c reductase activity determined as described in Materials and Methods; 100% refers to the cyt bc_1 activity [1.74 μmol of cyt c reduced min^{-1} (mg of total membrane proteins)$^{-1}$] exhibited by cells harboring pMTS1. Note the variability of the values obtained which is consistent with the lability of heterodimeric enzymes. [d]$E_{m,7}$ refers to the redox midpoint potentials of hemes b_L, b_H, and c_1 approximated as described in Materials and Methods. [e]SS, FF, and FS denote homo- and heterodimeric cyt bc_1 variants assembled, and A−D refer to Figure 2. [f]Note that 13.2% would correspond to 12.4% by taking as 100% the activity observed with cells harboring pMTS1-S. Similarly, 9.2% would correspond to 11.5% by taking as 100% the activity observed with cells harboring pMTS1-F. [g]Not done. [h]Not applicable.

yielded Ps^+ revertants with similar frequencies of $\sim10^{-5}$ (data not shown). Inspections of cell populations harboring pED2 and pED3 indicated that more than 99.99% cells exhibited slow $Ps^{\pm}$ growth, which was distinct from the vigorous Ps^+ growth of rare revertants (< 0.01%) that occurred in the population (Figure 3A, top).

In agreement with the Ps phenotypes, chromatophore membranes of cells harboring pMTS1, pMTS1-S, and pMTS1-F plasmids had cyt bc_1 activities of ~1.74, ~1.85, and ~1.39 μmol of cyt c reduced min^{-1} (mg of total membrane proteins)$^{-1}$, respectively, whereas those with pED2 or pED3 yielded only 0.23 or 0.16 μmol of cyt c reduced min^{-1} (mg of total membrane proteins)$^{-1}$, respectively (~13 and 9% of the activity seen with wild-type pMTS1, respectively). Cells harboring two plasmids exhibited higher but somewhat variable (~22 to 15% of that of the wild type, partly because of enzyme lability) cyt bc_1 activities (Table 2), which could not be attributed to the rare revertants (at best forming 0.01% of the populations used). These data indicated that independent assortment of the two different variants of cyt b occurred in cells harboring two plasmids to yield functional heterodimeric cyt bc_1 variants in line with their slow Ps growth.

Additional analyses of chromatophore membranes by SDS−PAGE and immunoblots established that cells harboring pED2 and pED3 contained both cyt b-S and cyt b-F variants, and that the amounts of cyt b and cyt c_1 subunits detected using appropriate antibodies were similar to those observed with the corresponding wild-type strains (Figure 3B). Ascorbate or dithionite reduced minus ferricyanide oxidized optical difference spectra (Figure 3C) of chromatophore membranes were used to assess the amounts of total c-type and b-type cyts in different strains. As expected, the wild-type parent (pMTS1) and the cyt b-S:Y147A (pED2) mutant had more 560 nm-absorbing material than 550 nm-absorbing material attributed to the b- and c-type cyts, respectively. The cyt b-F:H212N (pED3) mutant showed the opposite pattern, in agreement with its missing heme b_H. Comparatively, membranes of cells harboring pED2 and pED3 had intermediate amounts of b- and c-type cyts, seemingly producing cyt bc_1 variants with different amounts of heme b_H (Figure 3C,D). Dark equilibrium redox titrations using membranes derived from appropriate strains verified the thermodynamic properties of heme b_L, b_H, and c_1 cofactors of cyt bc_1 (Table 2). In these experiments, wild-type cyt bc_1 (pMTS1) displayed $E_{m,7}$ values of −133, 67, and 310 mV for heme b_L, b_H, and c_1 cofactors, respectively. We note that these values appear to be slightly higher than those routinely observed, possibly because of the experimental conditions used here. The homodimeric cyt bc_1 mutant variants cyt b-S:Y147A and cyt b-F:H212N resulted in values of −137, 70, and 305 mV and values of −145, (62), and 300 mV for the heme b_L, b_H, and c_1 cofactors, respectively. Similar $E_{m,7}$ values were obtained with membranes of cells harboring pED2 and pED3 (−147, 73, and 300 mV for heme b_L, b_H, and c_1 cofactors, respectively). We note that these $E_{m,7}$ values should be considered approximate, especially in light of heterogeneous cyt bc_1 subpopulations in the membranes of these strains. The identity of cyt b species exhibiting an $E_{m,7}$ value of (~60) mV in membranes of cells harboring pED3 (cyt b-F:H212N) is unknown, but it does not correspond to heme b_H, which is missing in this mutant (see EPR studies below and the Supporting Information). In any event, no major difference was seen among the $E_{m,7}$ values of the heme b_H (when present), b_L, and c_1 cofactors of the homo- and heterodimeric cyt bc_1 variants (Table 2). However, note that these experiments could not determine whether the two b_L hemes of a heterodimeric cyt bc_1 variant have identical or different $E_{m,7}$ values.

The cofactors associated with cyt bc_1 were also analyzed using EPR spectroscopy, especially to monitor hemes b_L and b_H, and the [2Fe-2S] cluster of cyt bc_1 in various mutants (Figure 3D,E). EPR resonance lines 3.78 and 3.43 corresponding to the g_z features of oxidized hemes b_L and b_H, respectively, were detected in membranes derived from cells producing the wild type (pMTS1) and cyt b-S:Y147A variant (pED2) (*39*). Cells with the cyt b-F:H212N variant (pED3) lacked the g_z feature at 3.43, while those harboring pED2 and pED3 had both of the g_z features at 3.78 and 3.43. However, the amplitudes and shapes of the latter EPR spectra were distinct from those of a wild-type strain (Figure 3D). EPR dark equilibrium redox titrations of hemes b_L and b_H of cyt bc_1 were conducted to prevent any overlap with interfering component(s) with similar optical properties

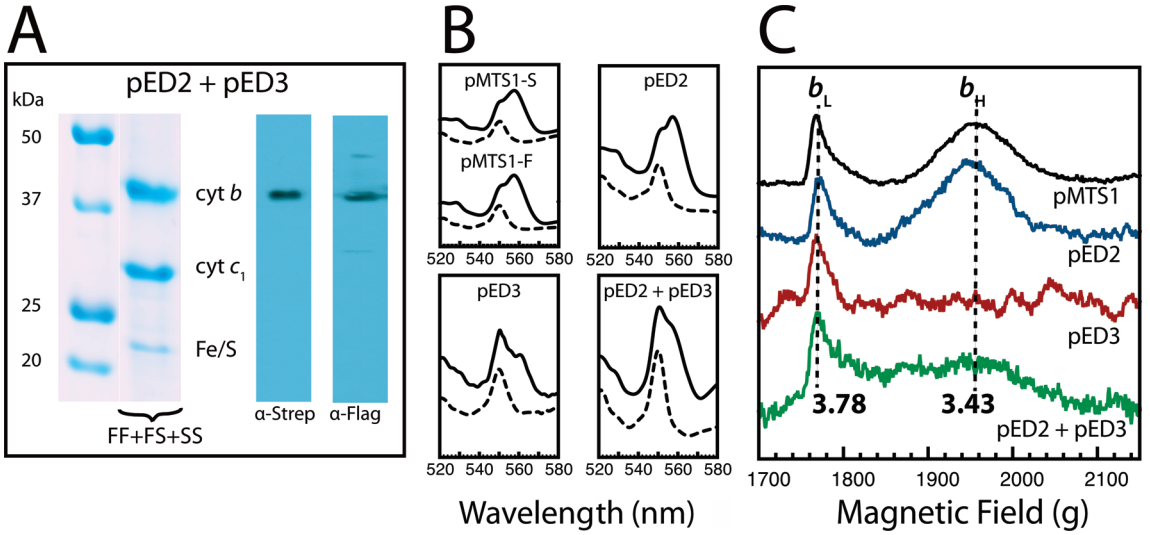

FIGURE 4: Biochemical properties of partially purified *R. capsulatus* cyt *b*-S:Y147A−cyt *b*-F:H212N heterodimeric cyt bc_1 variants. (A) Homodimeric (FF and SS) and heterodimeric (FS) cyt bc_1 variants purified from cells harboring pED2 and pED3 by DEAE-Biogel A chromatography were analyzed by SDS−PAGE (12.5%) and immunoblots using approximately 5 μg of proteins and anti-Strep II (α-Strep) or anti-Flag M2 (α-Flag) monoclonal antibodies. Fe-S protein, cyt *b*, and cyt c_1 subunits of cyt bc_1 are indicated. Note that Flag-tagged (pMTS1-F) and Strep-tagged (pMTS1-F) wild type and homodimeric cyt *b*-S:Y147A (pED2) and cyt *b*-F:H212N (pED3) cyt bc_1 variants were also purified but are not shown for the sake of clarity. (B) Total *b*-type and *c*-type cyt content of purified materials obtained from appropriate *R. capsulatus* strains (as described in the legend of Figure 2A) used to determine their ascorbate (---) or dithionite (—) reduced minus ferricyanide oxidized optical difference spectra. Note that these spectra are similar to those obtained using appropriate chromatophore membranes shown in Figure 3C. (C) Low-spin heme EPR spectra of purified materials obtained from appropriate *R. capsulatus* strains (as described in the legend of Figure 2A). All samples were oxidized directly in the EPR tube via addition of 5 μL of 10 mM ferricyanide. The experimental conditions were as described in the legend of Figure 3D, and a "nonsignal" portion of a baseline spectrum simulated by a third-order polynomial fit was subtracted as a baseline correction.

(Figure S1A,B of the Supporting Information). These measurements indicated that hemes b_L and b_H that were detectable in membranes from cells harboring pED2 and pED3 producing heterodimeric cyt bc_1 variants had $E_{m,7}$ values comparable to those determined by optical titrations (Table 2 and Supporting Information). The EPR spectra of the Fe-S protein subunit of cyt bc_1 were also monitored. The Fe-S protein was present in similar amounts in all cases, as deduced from the g_y transition amplitudes of the reduced [2Fe-2S] clusters (Figure 3E). The shape and g_x (1.804) values of the Fe-S protein [2Fe-2S] cluster signals were identical in all mutants, indicating that the Q_o site Q/QH_2 occupancies of all cyt bc_1 variants were comparable. Overall, the data established that all strains, including those harboring pED2 and pED3, produced the expected cyt bc_1 mutant variants in similar amounts.

Purification and Characterization of Epitope-Tagged Homodimeric cyt bc_1 Variants. The properties of cells harboring pED2 and pED3 enticed us to seek direct physical evidence of the occurrence of active heterodimeric cyt bc_1 species under appropriate conditions. A two-step purification method, starting with anion exchange chromatography with a DEAE-Biogel A column (*15*) followed by epitope tag affinity chromatography, yielded large quantities of purified, epitope-tagged wild-type (pMTS1-S and pMTS1-F) and single-mutant (pED2 and pED3) cyt bc_1 homodimers for biochemical characterizations (Table 2, Figure 4A, data and not shown). Purified wild-type Strep-tagged (pMTS1-S) and Flag-tagged (pMTS1-F) cyt bc_1 had activities of 8.3 and 7.7 μmol of cyt *c* reduced min^{-1} (mg of total proteins)$^{-1}$, respectively. In contrast, purified mutant cyt *b*-S:Y147A (pED2) and cyt *b*-F:H212N (pED3) variants had ~10-fold lower activities of 0.8 and 0.5 μmol of cyt *c* reduced min^{-1} (mg of total proteins)$^{-1}$, respectively. SDS−PAGE and immunoblots with cyt *b* and epitope tag antibodies, as well as optical and EPR spectral analyses (Figure 4B,C), indicated that the properties of purified, epitope-tagged homodimeric cyt bc_1 variants were comparable to those of their membrane-embedded versions. Only the cyt *b*-F:H212N (pED3) variant lacking heme b_H was unstable and aggregated rapidly. This mutant enzyme did not bind tightly to the DEAE-Biogel A column at salt concentrations of >150 mM NaCl, rendering its purification difficult, in contrast to the other variants that remained bound at salt concentrations of up to 350 mM.

Physical Evidence of the Production of a Heterodimeric cyt bc_1 in R. capsulatus. Despite the difficulties encountered with the cyt *b*-F:H212N mutant, we purified epitope-tagged heterodimeric cyt bc_1 variants from cells harboring pED2 and pED3 by DEAE-Biogel A chromatography followed by two consecutive affinity chromatography steps. DEAE-Biogel A chromatography yielded partially purified and active epitope-tagged cyt bc_1 [~2 μmol of cyt *c* min^{-1} (mg of total proteins)$^{-1}$] with expected optical and EPR spectra (Figure 4). These preparations were expected to contain both homodimeric (called SS and FF for cyt *b*-S:Y147A and cyt *b*-F:H212N, respectively) and heterodimeric (called FS for cyt *b*-S:Y147A−cyt *b*-F:H212N) cyt bc_1 populations. They were further fractionated into homodimeric (FF and SS) and heterodimeric (FS) cyt bc_1 variants by two consecutive affinity chromatography steps (Flag followed by Strep binding columns, and Strep followed by Flag binding columns) (Figure S2A,B of the Supporting Information). In both cases, final elution fractions contained highly enriched heterodimeric cyt *b*-S:Y147A−cyt *b*-F:H212N (FS) variants of cyt bc_1, which had no enzymatic activity. Nonetheless, the successful isolation of FS subpopulations by two consecutive affinity chromatography steps in either order confirmed the occurrence of heterodimeric cyt bc_1 species in cells harboring pED2 and pED3 plasmids (Supporting Information).

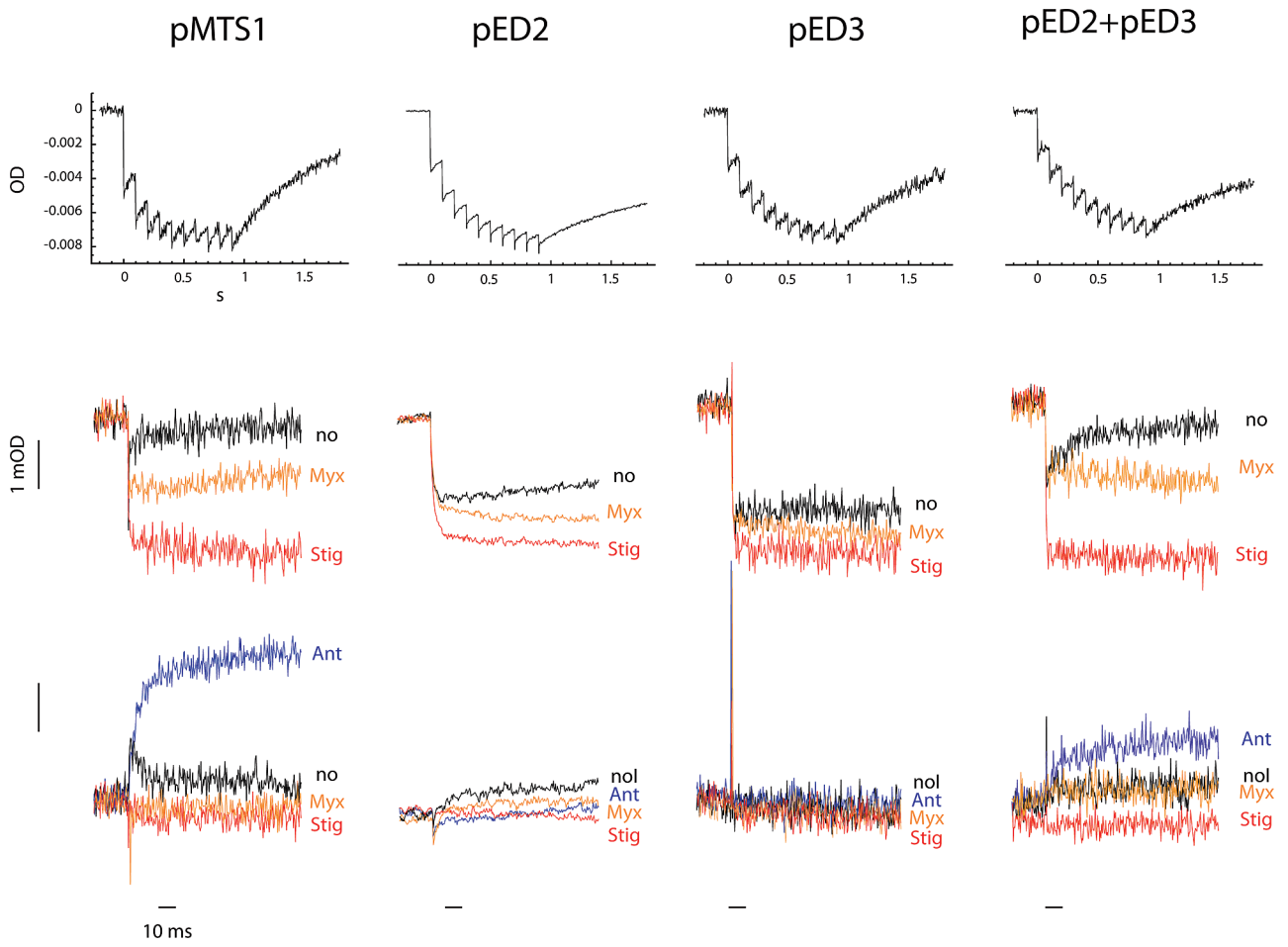

FIGURE 5: Light-induced, time-resolved cyt *b* reduction and cyt *c* re-reduction kinetics of various *R. capsulatus* strains. *R. capsulatus* strains harboring plasmids pMTS1 producing wild-type, pED2 and pED3 producing homodimeric cyt *b*-S:Y147A and cyt *b*-F:H212N, respectively, and pED2+pED3 producing heterodimeric cyt *b*-S:Y147A−cyt *b*-F:H212N cyt bc_1 variants were analyzed. In each case, chromatophore membranes corresponding to an amount of RC equal to 0.30 μM were resuspended in 50 mM MOPS buffer (pH 7.0) containing 100 mM KCl at an E_h of 100 mV. The exact amount of RC was determined from the extent of its photo-oxidation after a train of 10 flashes, separated by 50 ms at an E_h of 380 mV (top panel) and an extinction coefficient of 29 mM^{-1} cm^{-1} at 605 nm minus 540 nm, as described in Materials and Methods. In all samples, cyt *c* re-reduction kinetics (middle panel) were monitored at 550 nm minus 540 nm, in the absence of inhibitor (no), or in the presence of 10 μM myxothiazol (Myx), which abolishes QH_2 oxidation at the Q_o site, or 10 μM stigmatellin (Stig), which abolishes the transfer of an electron from the [2Fe-2S] cluster to heme c_1 by immobilizing the head domain of the Fe-S protein subunit at the Q_o site. Similarly, cyt *b* reduction kinetics (bottom panel) were monitored at 560 nm minus 570 nm, in the absence of inhibitor (no), or in the presence of 10 μM Q_i site inhibitor antimycin (Ant). Note that the samples of pED2 were analyzed using slightly different equipment, which yielded a signal-to-noise ratio higher than those of the other samples.

Light-Activated, Single-Turnover cyt c and cyt b Reduction Kinetics of Homo- and Heterodimeric R. capsulatus cyt bc_1. The slow Ps growth ability of cells harboring pED2 and pED3 plasmids indicated that they conducted photosynthetic cyclic electron transport upon light activation. The cyt *c* and cyt *b* reduction kinetics were monitored using chromatophore membranes derived from cells harboring homo- or heterodimeric cyt bc_1 variants using light-activated, time-resolved optical kinetic spectroscopy (Figure 5). Chromatophore membranes of various strains were normalized per amount of photochemical reaction center (RC) that they contained (Figure 5, top panel). Millisecond time scale cyt *c* (Figure 5, middle panel) and cyt *b* (Figure 5, bottom panel) reduction kinetics were monitored at an ambient potential (E_h) of 100 mV with the wild type (pMTS1) as well as the homodimeric and heterodimeric cyt bc_1 variants (pED2, pED3, and pED2+pED3). As expected, chromatophore membranes of the wild-type strain exhibited submillisecond time scale oxidation, followed by cyt *c* re-reduction kinetics in the millisecond range (*40*). Addition of myxothiazol or stigmatellin inhibited the cyt *c* re-reduction kinetics partly or completely, respectively (Figure 5, left column, middle row). Stigmatellin revealed the full extent of cyt *c* oxidation by inhibiting Q_o site catalysis and immobilizing the Fe-S protein head domain at this site, while myxothiazol inhibited only QH_2 oxidation, leaving the Fe-S protein head domain mobile (*8*). Fast cyt *c* re-reduction kinetics were not seen in membranes derived from cells carrying either pED2 or pED3, even in the absence of inhibitor, in agreement with their lacking an active cyt bc_1 (Figure 5, two middle columns, middle rows). Membranes of cells harboring the cyt *b*-S:Y147A (pED2) variant exhibited reduction kinetics slightly faster than those seen with cyt *b*-F:H212N (pED3), and these kinetics were fully inhibited upon addition of inhibitors, as reported previously (*32*). The extents of cyt *c* oxidation seen with inactive cyt bc_1 mutants in the absence of inhibitor were almost similar to those observed with wild-type cyt bc_1 in the presence of inhibitors. Thus, these mutants did not contain active cyt bc_1 species, in agreement with their Ps^- phenotype. Interestingly, membranes of cells harboring pED2 and pED3 exhibited cyt *c* re-reduction kinetics that were faster than those carrying pED2 or pED3 but slower than those seen with membranes from wild-type

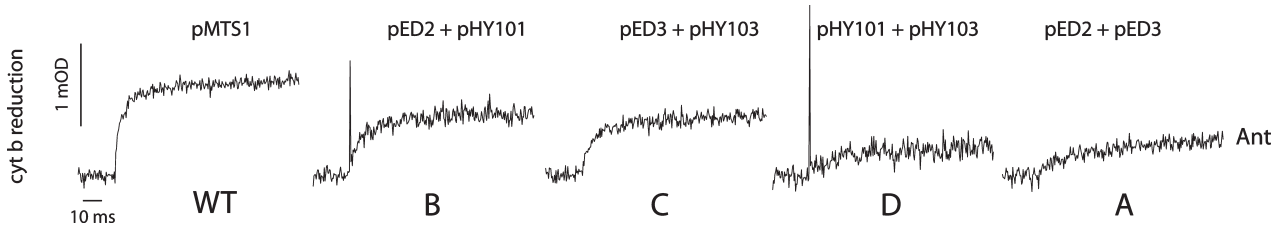

FIGURE 6: Light-induced, time-resolved cyt *b* reduction kinetics exhibited by *R. capsulatus* strains harboring different plasmid combinations yielding heterodimeric cyt bc_1 variants. The cyt *b* reduction kinetics were monitored using chromatophore membranes prepared from appropriate cells (pMTS1, pED2+pED3, pED2+pHY101, pED3+pHY103 and pHY101+pHY103) grown in enriched medium under respiratory growth conditions. All plasmid combinations (A−D) are described in the legend of Figure 2 and Table 1. Experimental conditions were as described in the legend of Figure 5, using chromatophore membranes containing 0.30 μM RC, appropriate mediators (Materials and Methods), 3 μM valinomycin, and 10 μM antimycin A. Samples were poised at 100 mV. Note that the extent and rate of cyt *b* reduction change depending on the strains, with cells harboring identical replicons exhibiting more pronounced kinetics, possibly reflecting better electronic couplings in membranes harboring heterogeneous cyt bc_1 subpopulations.

cyt bc_1-producing cells (Figure 5, right column, middle row). In all cases, the cyt *c* re-reduction kinetics were sensitive to myxothiazol and stigmatellin (*38*), indicating that they reflected cyt bc_1 specific activities. Kinetic patterns similar to cyt *c* re-reduction kinetics were also observed with cyt *b* reduction kinetics (Figure 5, bottom panel). Upon addition of antimycin A, which eliminates the transfer of an electron from cyt b_H to Q at the Q_i site, rapid cyt *b* reduction was seen with membranes derived from cells producing wild-type cyt bc_1, but not with those that have a defective enzyme lacking heme b_H (pED3), or an extremely slow Q_o site catalysis (pED2). In the presence of antimycin A, membranes from cells harboring pED2 and pED3 exhibited readily detectable cyt *b* reduction kinetics, although these kinetics were slower and had amplitudes smaller than those seen with membranes from cells producing wild-type cyt bc_1 (Figure 5, right vs left columns, bottom row). In all cases, the cyt *b* reduction kinetics were sensitive to the Q_o site inhibitors myxothiazol and stigmatellin, confirming that they originated from Q_o site catalysis. The cyt *c* re-reduction and cyt *b* reduction kinetics seen with membranes of cells harboring the cyt *b*-S:Y147A−cyt *b*-F:H212N variants of cyt bc_1 (pED2+pED3) established that the heterodimeric enzymes were active and able to sustain cyclic electron transport between the RC and cyt bc_1 to support Ps growth. As the homodimeric enzymes are inactive, we concluded that heterodimeric cyt bc_1 variants effectively conduct electron transfer between the b_L hemes of their two monomers (Figure 2B, middle panel).

The Extent of cyt b Reduction Depends on the Amount of Heterodimeric cyt bc_1 Present in Cells. As different plasmids with different replication properties yielded different amounts of heterodimeric cyt bc_1 based on SDS−PAGE and immunoblot data, we examined membranes derived from cells harboring the four different combinations (A, B, C, and D) of plasmids (Figure 2C) producing heterodimeric cyt bc_1 variants. The extents of cyt *b* reduction were monitored in the presence of antimycin A using membrane preparations normalized per amount of RC (Figure 6). The data indicated that membranes from cells harboring identical plasmids (i.e., pRK-type pED2+pHY101, or composite pED3+pHY103) exhibited more pronounced cyt *b* reduction and cyt *c* re-reduction kinetics. Under identical light activation conditions, the detection of larger extents of cyt *b* kinetics per amount of RC suggested that larger amounts of heterodimeric cyt bc_1 were electronically coupled to the RCs. These experiments documented that the new genetic system used here has the ability to produce different amounts of heterodimeric cyt bc_1 variants, changing the coupling ratios between the physiological Ps electron transport partners in chromatophore membranes.

DISCUSSION

Static three-dimensional structural models often depict cyt bc_1 as a dimer of two identical monomers (*8*−*11*, *22*) (Figure 1). However, the mobility of the Fe-S protein subunit during hydroquinone oxidation at the Q_o site indicates that the enzyme undergoes large conformational changes during its catalytic turnover (*41*). These considerations led us to the "heterodimeric modified Q cycle" model (*26*), which was reviewed recently by Cooley (*42*). In our work, we developed a new genetic system for examining intra- and intermonomer interactions in cyt bc_1 and used it to test the occurrence of intermonomer electron transfer between the b_L hemes of this enzyme. We thought that if a heterodimeric cyt bc_1 with only one active Q_o site in one monomer and one active Q_i site in the other monomer is obtained by coexpression of two *petABC* operons, then intermonomer electron transfer between the b_L hemes could be probed. However, neither the degree of recombination in vivo that might occur between homologous copies of *petABC* carried by two plasmids nor which specific mutation(s) to use to inactivate the Q_o and Q_i sites was known (*6*). We found that the Ps^+ reversion rates observed in cells harboring two similar plasmids, comaintained using two antibiotic resistance markers, were not exorbitantly high as compared with those carrying only one plasmid. To avoid the mutations that affect the occupancy of the Q binding sites or those that immobilize the Fe-S protein head domain, we opted for the cyt *b*:Y147A and cyt *b*:H212N mutations that we had characterized previously (*12*, *32*). To the best of our knowledge, the heterodimeric cyt bc_1 obtained in this work (Figure 7) is the first example of such an enzyme that is sufficiently active to sustain Ps growth. This cyt bc_1 variant remains active, conserves its subunit stoichiometry upon detergent solubilization and DEAE-Biogel A chromatography, but loses its activity during subsequent affinity purification. Matrix-induced inactivation observed with wild-type *R. capsulatus* cyt bc_1 (*15*) might account for the loss of activity. However, as Strep-tagged wild-type and cyt *b*-S:Y147A enzymes were readily purified without loss of activity using the same columns, the observed instability and the poor DEAE-Biogel A binding properties of the heterodimeric cyt *b*-S:Y147A−cyt *b*-F:H212N variant are probably due to the intrinsic instability of cyt bc_1 in the absence of its heme b_H. The four-helix bundle that coordinates hemes b_L and b_H defines the interface between the two monomers and is a key feature for the

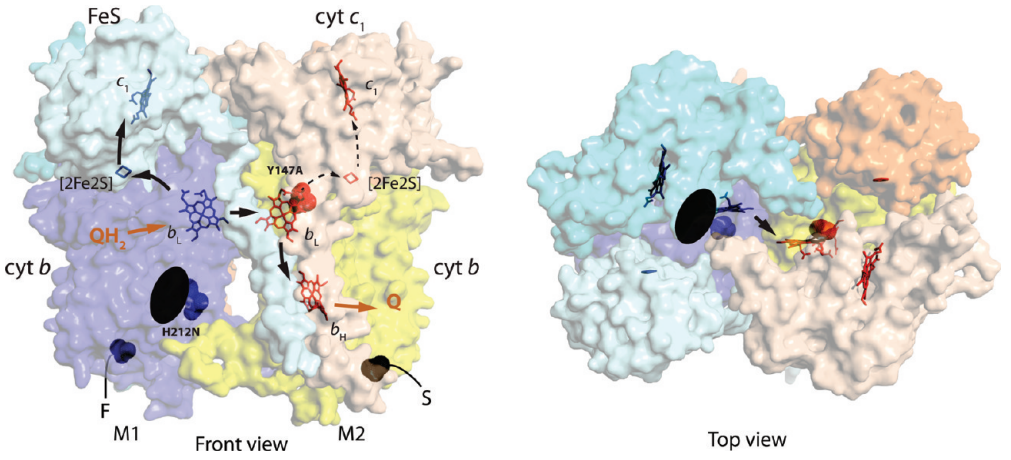

FIGURE 7: Model depicting intermonomer electron transfer between the hemes b_L of monomers in a heterodimeric cyt bc_1. The three-dimensional structure (PDB entry 1ZRT) of *R. capsulatus* cyt bc_1 shown in Figure 1 is modified to show the location and nature of the mutations used in this work, revealing intermonomer electron transfer between the heme b_L cofactors of the enzyme. All structural features are as in Figure 1, except that the cyt *b*:Y147A and cyt *b*:H212N substitutions are shown as space filling models in blue on M1 and red on M2 monomers. The absence of heme b_H in one monomer, due to the latter mutation, is indicated by a black ellipsoid, and the residual electron transfer that is unable to support Ps growth but still occurs in the presence of the former mutation is indicated by dotted arrows. The thick black arrows correspond to the productive intermonomer electron transfer that occurs across the functional Q_o and Q_i sites of the heterodimeric cyt bc_1. Note that this electron transfer is efficient enough to support Ps growth of *R. capsulatus* but apparently is rate-limiting because it can confer only a slow $Ps^{\pm}$ growth phenotype.

dimeric architecture of cyt bc_1 (*11*). While embedding a mutant enzyme in the membrane lipid bilayer appears to compensate for the loss of heme b_H by preventing its disassembly, progressive loss of enzyme activity and partial dissociation of the monomers occur upon detergent dispersion and render purification difficult.

Our earlier works on subunit maturation and assembly of *R. capsulatus* cyt bc_1 (*14*, *43*) indicated that the Fe-S protein, cyt *b*, and cyt c_1 subunits follow independent pathways for prosthetic group acquisition and maturation to yield a stable cyt bc_1 subcomplex to which the Fe-S protein subunit could be added even in vitro (*15*). How the monomers dimerize to form the active enzyme is unknown. Our finding that coexpression of two inactive cyt bc_1 species yields an active heterodimeric variant with distinct features suggests that cyt bc_1 monomers, or their subunits, associate independently to yield homo- and heterodimeric cyt bc_1 variants. A likely possibility is the association of cyt *b* and cyt c_1 into a cyt bc_1 dimeric subcomplex followed by the addition of two Fe-S protein subunits to form the active dimeric cyt bc_1 (*14*). Whether first the complete monomers are formed, and then are dimerized, might be tested using the genetic system described in this work to further elucidate the biogenesis process of cyt bc_1.

An important finding of this work is that, under appropriate conditions, intermonomer electron transfer occurs between the b_L hemes of cyt bc_1 monomers (Figure 7) and also the rate and efficiency of this event are sufficiently high to sustain physiological Ps growth of *R. capsulatus*. The cyt *b* reduction kinetics in the presence of antimycin A at an E_h of 100 mV observed with the heterodimeric cyt bc_1 variants were slower than the similar kinetics seen with a wild-type enzyme. Note that the measured cyt *b* reduction rates in the presence of antimycin A encompass multiple, indirectly coupled steps, and in some cases (e.g., A and D constructs), the signal-to-noise ratio is poor, rendering them less reliable. Nonetheless, semiquantitative estimations of these rates (by curve fitting to a single-exponential equation) (Figure 6) suggested that while the wild-type membranes exhibited rates of $\sim$325 s^{-1}, those containing heterodimeric cyt bc_1 rates ranged from 55−60 s^{-1} (A and D constructs) to 150−180 s^{-1} (B and C constructs). In any event, in heterodimeric cyt bc_1 variants, intermonomer hemes $b_L-b_L-b_H$ electron transfer rates are comparatively slower than intramonomer heme b_L-b_H electron transfer rates (Figure 7). Moreover, depending on the amounts of heterodimeric variants, more cyt *c* (cyt c_2 and c_y)-dependent cyt bc_1 to RC cyclic electron transfer was observed upon light activation of a given amount of RC. Strains producing larger amounts of heterodimeric enzymes exhibited more pronounced cyt *b* and cyt *c* reduction kinetics, possibly improving RC−cyt c_y/c_2−cyt bc_1 coupling to better support Ps growth. Future studies producing different heterodimeric cyt bc_1 variants will further address these issues in detail.

Studies similar to those described in this work have been reported recently (*29*, *30*). The work with *Paracoccus denitrificans* used two plasmids to coexpress a native and a Q_o site-defective cyt bc_1 variant that were tagged by two different epitope tags to purify and analyze the homo- and heterodimeric enzymes produced. It was reported that a purified heterodimeric cyt bc_1 with only one active Q_o site was as active as a native enzyme with two active Q_o sites on the time scales used, and considered to reflect intermonomer electron transfer (*30*). A second related work used a modified *petABC*, where *pet*B encoding cyt *b* was duplicated and the two copies were linked in-frame using a small exogenous sequence encoding a dodecapeptide, and a carboxyl-terminal epitope tag was added to facilitate purification (*29*). This construct yielded a non-native cyt bc_1-like enzyme akin to a cyt bc_1 dimer with its two cyt *b* subunits substituted with a covalently linked "cyt *b*−cyt *b*" hybrid. Intermonomer electron transfer among hemes b_L, b_L, and b_H of this artificial cyt bc_1-like enzyme was shown to occur using an appropriately mutated cyt *b*−cyt *b* fusion subunit and light-activated kinetic spectroscopy (*29*). The Ps growth ability and reversion rate of these mutants as well as the subunit stoichiometry, dimeric state, or three-dimensional structures of these enzymes have not been reported (*29*). Comparisons of the properties of the artifical cyt bc_1-like variants harboring two fused cyt *b* with the more nativelike heterodimeric cyt bc_1 enzymes as reported in this work would be informative.

Experimental observation of intermonomer electron transfer (Figure 7) is highly significant with respect to the heterodimeric Q cycle model, which postulates dismutation of the two SQ

molecules that accumulated at the Q_i sites to Q and QH_2 to initiate the next turnover of cyt bc_1 (*26*). Recently, Cooley has discussed structural elements of cyt *b* that might govern Q_o-Q_i site interactions across the membrane, such as the formation of SQ at one of the Q_i sites allowing the cognate Q_o site *ef* loop to act as a temporal "gate" for the initiation of the next QH_2 oxidation (*42*). If such a gate exists, then how long this gate remains "closed" might depend on how stable the SQ is at the Q_i site. Q_i site mutants with increased SQ K_{stab} at the Q_i site, like the cyt *b*: H217R substitutions, produce functional but less active homodimeric cyt bc_1 variants (*38*), suggesting that extreme stability of SQ may be required to inactivate cyt bc_1 completely. In agreement with this suggestion, a fused cyt *b*−cyt *b* hybrid containing cyt bc_1-like enzyme formed from one fully active and one both Q_o and Q_i site inactive monomers apparently remains active (*29*). Undoubtedly, the ongoing use of different genetic systems that produce heterodimeric cyt bc_1 variants would be invaluable in assessing the validity of current catalytic models invoking dimeric cyt bc_1.

ACKNOWLEDGMENT

We thank N. Selamoglu for critical reading of the manuscript and acknowledge the Johnson Research Foundation for use of EPR and kinetic spectroscopy facilities, without which this work would have been impossible. We also thank Drs. P. L. Dutton and C. Moser for their help.

SUPPORTING INFORMATION AVAILABLE

EPR dark equilibrium redox titrations of hemes b_L and b_H of heterodimeric cyt bc_1 variants using chromatophore membranes (Figure S1A,B) and physical evidence of the production of heterodimeric cyt bc_1 variants using DEAE-Biogel A chromatography followed by two consecutive affinity chromatography steps (Figure S2A,B). This material is available free of charge via the Internet at http://pubs.acs.org.

REFERENCES

1. Berry, E. A., Guergova-Kuras, M., Huang, L. S., and Crofts, A. R. (2000) Structure and function of cytochrome *bc* complexes. *Annu. Rev. Biochem. 69*, 1005–1075.
2. Mitchell, P. (1976) Possible molecular mechanisms of the protonmotive function of cytochrome systems. *J. Theor. Biol. 62*, 327–367.
3. Trumpower, B. L. (1990) The protonmotive Q cycle. Energy transduction by coupling of proton translocation to electron transfer by the cytochrome bc_1 complex. *J. Biol. Chem. 265*, 11409–11412.
4. Daldal, F., Davidson, E., and Cheng, S. (1987) Isolation of the structural genes for the Rieske Fe-S protein, cytochrome *b* and cytochrome c_1 all components of the ubiquinol:cytochrome c_2 oxidoreductase complex of *Rhodopseudomonas capsulata*. *J. Mol. Biol. 195*, 1–12.
5. Atta-Asafo-Adjei, E., and Daldal, F. (1991) Size of the amino acid side chain at position 158 of cytochrome b is critical for an active cytochrome bc1 complex and for photosynthetic growth of *Rhodobacter capsulatus*. *Proc. Natl. Acad. Sci. U.S.A. 88*, 492–496.
6. Berry, E. A., Lee, D.-W., Huang, L.-S., and Daldal, F. (2009) Structural and Mutational Studies of the cytochrome bc_1 complex. In The Purple Phototrophic Bacteria (Hunter, C. N., Daldal, F., Thurnauer, M. C., and Beatty, J. C., Eds.) pp 425−450, Springer, Berlin.
7. Lee, D. W., Ozturk, Y., Osyczka, A., Cooley, J. W., and Daldal, F. (2008) Cytochrome bc_1-c_y fusion complexes reveal the distance constraints for functional electron transfer between photosynthesis components. *J. Biol. Chem. 283*, 13973–13982.
8. Zhang, Z., Huang, L., Shulmeister, V. M., Chi, Y. I., Kim, K. K., Hung, L. W., Crofts, A. R., Berry, E. A., and Kim, S. H. (1998) Electron transfer by domain movement in cytochrome bc_1. *Nature 392*, 677–684.
9. Xia, D., Yu, C. A., Kim, H., Xia, J. Z., Kachurin, A. M., Zhang, L., Yu, L., and Deisenhofer, J. (1997) Crystal structure of the cytochrome bc_1 complex from bovine heart mitochondria. *Science 277*, 60–66.
10. Iwata, S., Lee, J. W., Okada, K., Lee, J. K., Iwata, M., Rasmussen, B., Link, T. A., Ramaswamy, S., and Jap, B. K. (1998) Complete structure of the 11-subunit bovine mitochondrial cytochrome bc_1 complex. *Science 281*, 64–71.
11. Berry, E. A., Huang, L. S., Saechao, L. K., Pon, N. G., Valkova-Valchanova, M., and Daldal, F. (2004) X-ray Structure of *Rhodobacter capsulatus* Cytochrome bc_1: Comparison with its Mitochondrial and Chloroplast Counterparts. *Photosynth. Res. 81*, 251–275.
12. Darrouzet, E., Valkova-Valchanova, M., Moser, C. C., Dutton, P. L., and Daldal, F. (2000) Uncovering the [2Fe2S] domain movement in cytochrome bc_1 and its implications for energy conversion. *Proc. Natl. Acad. Sci. U.S.A. 97*, 4567–4572.
13. Darrouzet, E., Valkova-Valchanova, M., and Daldal, F. (2000) Probing the role of the Fe-S subunit hinge region during Q_o site catalysis in *Rhodobacter capsulatus* bc_1 complex. *Biochemistry 39*, 15475–15483.
14. Davidson, E., Ohnishi, T., Tokito, M., and Daldal, F. (1992) *Rhodobacter capsulatus* mutants lacking the Rieske FeS protein form a stable cytochrome bc_1 subcomplex with an intact quinone reduction site. *Biochemistry 31*, 3351–3358.
15. Valkova-Valchanova, M. B., Saribas, A. S., Gibney, B. R., Dutton, P. L., and Daldal, F. (1998) Isolation and characterization of a two-subunit cytochrome b-c_1 subcomplex from *Rhodobacter capsulatus* and reconstitution of its ubihydroquinone oxidation (Q_o) site with purified Fe-S protein subunit. *Biochemistry 37*, 16242–16251.
16. Zara, V., Conte, L., and Trumpower, B. L. (2007) Identification and characterization of cytochrome bc_1 subcomplexes in mitochondria from yeast with single and double deletions of genes encoding cytochrome bc_1 subunits. *FEBS J. 274*, 4526–4539.
17. Crofts, A. R., Meinhardt, S. W., Jones, K. R., and Snozzi, M. (1983) The role of the quinone pool in the cyclic electron transfer chain of *Rhodopseudomonas sphaeroides*: A Modified Q-cycle mechanism. *Biochim. Biophys. Acta 723*, 202–218.
18. Osyczka, A., Moser, C. C., and Dutton, P. L. (2005) Fixing the Q cycle. *Trends Biochem. Sci. 30*, 176–182.
19. Gopta, O. A., Feniouk, B. A., Junge, W., and Mulkidjanian, A. Y. (1998) The cytochrome bc_1 complex of *Rhodobacter capsulatus*: Ubiquinol oxidation in a dimeric Q-cycle? *FEBS Lett. 431*, 291–296.
20. Trumpower, B. L. (2002) A concerted, alternating sites mechanism of ubiquinol oxidation by the dimeric cytochrome bc_1 complex. *Biochim. Biophys. Acta 1555*, 166–173.
21. Crofts, A. R., Holland, J. T., Victoria, D., Kolling, D. R., Dikanov, S. A., Gilbreth, R., Lhee, S., Kuras, R., and Kuras, M. G. (2008) The Q-cycle reviewed: How well does a monomeric mechanism of the bc_1 complex account for the function of a dimeric complex? *Biochim. Biophys. Acta 1777*, 1001–1019.
22. Solmaz, S. R., and Hunte, C. (2008) Structure of complex III with bound cytochrome *c* in reduced state and definition of a minimal core interface for electron transfer. *J. Biol. Chem. 283*, 17542–17549.
23. Covian, R., and Trumpower, B. L. (2005) Rapid electron transfer between monomers when the cytochrome bc_1 complex dimer is reduced through center N. *J. Biol. Chem. 280*, 22732–22740.
24. Gong, X., Yu, L., Xia, D., and Yu, C. A. (2005) Evidence for electron equilibrium between the two hemes b_L in the dimeric cytochrome bc_1 complex. *J. Biol. Chem. 280*, 9251–9257.
25. Cooley, J. W., Ohnishi, T., and Daldal, F. (2005) Binding dynamics at the quinone reduction Q_i site influence the equilibrium interactions of the iron sulfur protein and hydroquinone oxidation Q_o site of the cytochrome bc_1 complex. *Biochemistry 44*, 10520–10532.
26. Cooley, J. W., Lee, D. W., and Daldal, F. (2009) Across membrane communication between the Q_o and Q_i active sites of cytochrome bc_1. *Biochemistry 48*, 1888–1899.
27. Crofts, A. R., Barquera, B., Gennis, R. B., Kuras, R., Guergova-Kuras, M., and Berry, E. A. (1999) Mechanism of ubiquinol oxidation by the bc_1 complex: Different domains of the quinol binding pocket and their role in the mechanism and binding of inhibitors. *Biochemistry 38*, 15807–15826.
28. Osyczka, A., Moser, C. C., Daldal, F., and Dutton, P. L. (2004) Reversible redox energy coupling in electron transfer chains. *Nature 427*, 607–612.
29. Swierczek, M., Cieluch, E., Sarewicz, M., Borek, A., Moser, C. C., Dutton, P. L., and Osyczka, A. (2010) An electronic bus bar lies in the core of cytochrome bc_1. *Science 329*, 451–454.
30. Castellani, M., Covian, R., Kleinschroth, T., Anderka, O., Ludwig, B., and Trumpower, B. L. (2010) Direct demonstration of half-of-the-sites reactivity in the dimeric cytochrome bc_1 complex: Enzyme with one inactive monomer is fully active but unable to activate the second ubiquinol oxidation site in response to ligand binding at the ubiquinone reduction site. *J. Biol. Chem. 285*, 502–510.

31. Sambrook, J., and Russel, D. W. (2001) Molecular Cloning: A Laboratory Manual, 3rd ed., Cold Spring Harbor Laboratory Press, Plainview, NY.
32. Saribas, A. S., Ding, H., Dutton, P. L., and Daldal, F. (1995) Tyrosine 147 of cytochrome *b* is required for efficient electron transfer at the ubihydroquinone oxidase site (Q_o) of the cytochrome bc_1 complex. *Biochemistry 34*, 16004–16012.
33. Bolivar, F., Rodriguez, R. L., Greene, P. J., Betlach, M. C., Heyneker, H. L., Boyer, H. W., Crosa, J. H., and Falkow, S. (1977) Construction and characterization of new cloning vehicles. II. A multipurpose cloning system. *Gene 2*, 95–113.
34. Smith, P. K., Krohn, R. I., Hermanson, G. T., Mallia, A. K., Gartner, F. H., Provenzano, M. D., Fujimoto, E. K., Goeke, N. M., Olson, B. J., and Klenk, D. C. (1985) Measurement of protein using bicinchoninic acid. *Anal. Biochem. 150*, 76–85.
35. Laemmli, U. K. (1970) Cleavage of structural proteins during the assembly of the head of bacteriophage T4. *Nature 227*, 680–685.
36. Dutton, P. L. (1978) Redox potentiometry: Determination of midpoint potentials of oxidation-reduction components of biological electron-transfer systems. *Methods Enzymol. 54*, 411–435.
37. Saribas, A. S., Valkova-Valchanova, M., Tokito, M. K., Zhang, Z., Berry, E. A., and Daldal, F. (1998) Interactions between the cytochrome *b*, cytochrome c_1, and Fe-S protein subunits at the ubihydroquinone oxidation site of the bc_1 complex of *Rhodobacter capsulatus*. *Biochemistry 37*, 8105–8114.
38. Gray, K. A., Dutton, P. L., and Daldal, F. (1994) Requirement of histidine 217 for ubiquinone reductase activity (Q_i site) in the cytochrome bc_1 complex. *Biochemistry 33*, 723–733.
39. Salerno, J. C. (1984) Cytochrome electron spin resonance line shapes, ligand fields, and components stoichiometry in ubiquinol-cytochrome *c* oxidoreductase. *J. Biol. Chem. 259*, 2331–2336.
40. Robertson, D. E., Davidson, E., Prince, R. C., van den Berg, W. H., Marrs, B. L., and Dutton, P. L. (1986) Discrete catalytic sites for quinone in the ubiquinol-cytochrome c_2 oxidoreductase of *Rhodopseudomonas capsulata*. Evidence from a mutant defective in ubiquinol oxidation. *J. Biol. Chem. 261*, 584–591.
41. Darrouzet, E., Moser, C. C., Dutton, P. L., and Daldal, F. (2001) Large scale domain movement in cytochrome bc_1: A new device for electron transfer in proteins. *Trends Biochem. Sci. 26*, 445–451.
42. Cooley, J. W. (2010) A structural model for across membrane coupling between the Q_o and Q_i active sites of cytochrome bc_1. *Biochim. Biophys. Acta 1797*, 1842–1848.
43. Davidson, E., Ohnishi, T., Atta-Asafo-Adjei, E., and Daldal, F. (1992) Potential ligands to the [2Fe-2S] Rieske cluster of the cytochrome bc_1 complex of *Rhodobacter capsulatus* probed by site-directed mutagenesis. *Biochemistry 31*, 3342–3351.